THE INFLUENCE OF THERMAL RESIDUAL STRESSES AND FRICTION ON FATIGUE CRACK GROWTH IN FIBRE-REINFORCED INTERMETALLIC MATRIX COMPOSITES

G. Rauchs, P.F. Thomason, P.J. Withers

Manchester Materials Science Centre, University of Manchester,
Grosvenor Street, Manchester, M1 7HS, UK

ABSTRACT

A three-dimensional model of a compact tension specimen consisting of a Ti-6-4 matrix reinforced with unidirectional, continuous SiC fibres is investigated. The influence of post-processing thermal residual stresses and friction on the crack growth behaviour during monotonic and cyclic loading is assessed. It was found that the bridging fibres strongly reduce the crack-tip stress intensity factor. The thermal residual stresses produce a load of the crack tip in the absence of an external load and have an impact on the crack tip load ratio. The results are compared to investigations resulting from the modelling of crack-tip shielding by fibre-induced bridging tractions on the crack-face using the weight function method. Reasonable agreement was found between the two methods used.

KEYWORDS

Composites, Fibre reinforcement, Cyclic fatigue, Finite element modelling, Thermal residual stresses

INTRODUCTION

The relatively low fracture toughness in some metallic and intermetallic materials can often be improved by incorporating unidirectional fibre reinforcement [1-3]. One example is given by fibre-reinforced titanium matrix composites (TMCs) [2,3]. The cyclic fatigue of this material is also improved by the addition of unidirectional fibres to the matrix material. Experiments have shown that crack-tip shielding by fibre bridging can lead to crack arrest [2,3]. Several numerical studies have investigated the fracture behaviour of fibre reinforced materials, both for monotonic and cyclic loads [4-7]. Nevertheless most of these investigations rely heavily on the weight function method to assess the crack-tip shielding. This method is used within the context of continuum fracture mechanics wherein the bridging fibres are treated as a perturbation of the tractions acting on the faces of the matrix crack [5-9]. Therefore, the local traction transfer mechanism is smeared over the bridged area in the wake of the crack. Whereas elastic mismatch is accounted for in this approach, thermal expansion mismatch is mostly neglected. In recent years, finite element models of push-out tests have been developed to model the influence of debonding and friction on the material behaviour of fibre-reinforced materials [10,11]. Debonding has been modelled either by a quadratic failure criterion [11] or a Coulomb friction law [10], while interface friction has been included through the Coulomb friction law.

By using a finite element model, the mechanisms governing local stress transfer by bridging can be better resolved by modelling the individual bridging fibres and the fibre-matrix interface. The effects of elastic and thermal mismatch on fracture behaviour can also be investigated. In this study, this approach is used on a cracked compact tension specimen to investigate the cyclic fatigue behaviour of fibre-reinforced Ti-6Al-4V using a simple debonding criterion and friction model.

NUMERICAL MODELS

In the present study, a compact tension (CT) specimen of square shape with a sidelength of d=25 mm consisting of a Ti-6Al-4V matrix reinforced with continuous, unidirectional SiC-fibres normal to the crack surface is modelled using ABAQUS 5.8. The fibres have a diameter, d_f, of 0.1 mm and the fibre volume fraction f is 31%. Both matrix and fibres have purely linear-elastic material behaviour (Young's moduli E_m=115000 MPa, E_f=400000 MPa, Poisson's ratios ν_m=0.3, ν_f=0.17, CTE's α_m=10x10^{-6} 1/K, α_f=5x10^{-6} 1/K). Assuming that fibre bonding is weak, the debonding of the fibres is modelled by using the Coulomb friction law:

$$\tau \leq \mu \sigma_N \tag{1}$$

where τ is the interface shear stress, μ the friction coefficient and σ_N the normal compressive stress. Calculations for different interface strengths are performed by using different magnitudes for the friction coefficients μ. In order to model a true fibrous material rather than a layered composite, and to include the radial clamping stresses σ_N caused by thermal residual stresses and necessary for the debonding criterion used, a three-dimensional finite element analysis is necessary. Due to the small size of the fibres compared to the specimen, the size of the finite element model has been reduced considerably by using the embedded cell method. At the crack-tip, a microstructural region 20 fibres is modelled, while the remainder of the CT-specimen is modelled as a uniform continuum material with transversely isotropic material parameters representative of the composite properties. The growth of a crack around a fibre often leads to a curved crack front [12]. However here the model was simplified by assuming a straight crack at mid distance between two fibres, fully located in the matrix. The crack-tip stress intensity factor was calculated by the J-integral method. This is acceptable in our case for cyclic loads because of the linear-elastic behaviour of the matrix material. Because the stress intensity factor varies locally at the crack front, the average stress intensity factor was calculated from the values at each node on the crack front. In the model, crack growth is considered over a range of 10 fibres, with the crack length ranging from that of a half-cracked specimen +/- 5 fibres. This means that for the initial crack length a_0, 5 fibres remain in the wake of the crack and for the maximum crack length, 5 fibres remain in the unbroken ligament. This allows one to include the effects of the fibres for the minimum and maximum crack length and ensures that stress fluctuations from the transition from the embedded cell to the surrounding homogeneous bulk material do not seriously influence the magnitude of the stress intensity factor. It should be noted that the initial crack a_0 is unbridged, i.e. the fibres in the wake are cut. During crack growth, the fibres are assumed to remain intact and bridge the crack, with the crack growing only through the matrix.

The loads are applied in 3 steps. In the first step, the uncracked specimen is cooled down from the stress-free processing temperature to room temperature (ΔT=900K) to generate the initial residual stresses from the thermal expansion mismatch. In the second step, the initial crack, a_0, is introduced into the specimen by the node release technique. In the third step, the actual external load is applied. The magnitude of the external load is calculated in such a way as to obtain a constant applied stress intensity factor, K_{appl}, for all crack lengths using geometry functions Y(a/W) for CT-specimens taken from literature [13]. When considering cyclic loads, first the external load is applied, then the specimen is unloaded. The crack is then grown to the next crack location by the load release technique. This process is repeated until the maximum crack length is reached.

For the analytical model using the weight function method, the crack-tip stress intensity factor K_{tip} and the shielding K_{sh} have been calculated using a method of [8]. The bridging tractions, σ_{br}, including the effect of

thermal mismatch, are related to the crack-tip opening displacement u [9], using the fibre and matrix Young's modulus E_f and E_m, the fibre and matrix thermal expansion coefficient α_f and α_m, the temperature T with reference to the stress-free state, the rule-of-mixture Young's modulus E of the composite and a constant interface frictional stress τ, whose magnitude is derived by Eqn.1 from the interface pressure from the finite element results:

$$u = \frac{d_f(1-f^2)E_m^2}{4f^2E^2E_f\tau}\left[\sigma_{br} + f(E_f(\alpha_f - \alpha_m)T\right]^2 \tag{7}$$

The crack-tip opening displacement u at the location x on the crack with crack length a has been calculated using the weight function h(a,x) by:

$$u(x) = \frac{2}{E}\int_x^a h(a',x)\left[K_{appl}(a') + \int_{a_0}^{a'} h(a',x')\sigma_{br}(x')dx'\right]da' \tag{8}$$

In an iterative procedure, the crack-tip opening profile is calculated using Eqn.7 and 8. The crack tip stress intensity factor is calculated by using the applied crack tip stress intensity factor K_{appl} and the bridging stresses resulting from the crack-tip opening profile over the bridged crack length ranging from a_0 to a:

$$K_{tip} = K_{appl} + \int_{a_0}^a \sigma_{br}(x)h(a,x)dx \tag{9}$$

RESULTS

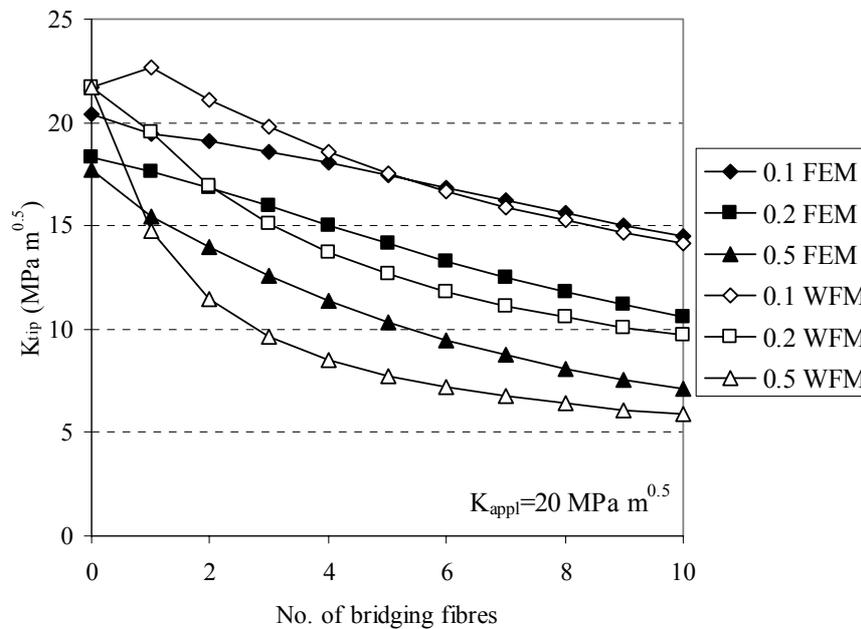*Effect of Thermal Residual Stresses*
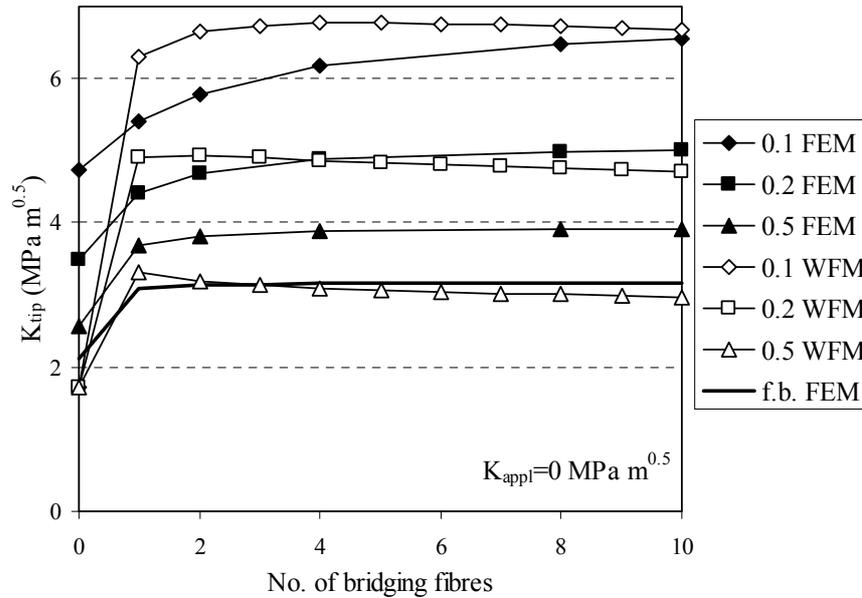
Figure 1: Comparison of results from finite elements and weight function method for thermal residual strains for several friction coefficients (0.1, 0.2 and 0.5).

It was found that after the cooling process, substantial thermal residual stresses occur in the composite. In the direction of the fibre axis, the fibres have a compressive stress of −899 MPa and the matrix has a tensile stress of 395 MPa. This is in good agreement with those measured by neutron diffraction (360 MPa in the

matrix and −720 MPa in the fibres [14]). After the introduction of the initial crack, the crack-tip experiences a considerable load resulting from the thermally induced residual stresses. It can be seen in Fig.1 that after crack growth, the thermally induced stress intensity factor, K_{th}, is magnified by the presence of one bridging fibre in the wake of the crack. The variation in stress intensity factor for different friction coefficients is caused by the varying debonding lengths of the non-bridging fibres, which increase as µ decreases. During further crack growth, the crack-tip stress intensity factor increases strongly for a friction coefficient µ=0.1, whereas for higher friction coefficients, the increase is small. It can be assumed that the bridging fibres inhibit the rotation of the crack face, which leads to an applied bending moment on the crack face resulting in an increase of the crack-tip stress intensity factor. This is underlined by the fact that the tensile stresses in the fibre are superimposed by bending stresses. This effect predominates in the case of one single bridging fibre. The increase of the crack-tip stress intensity factor with decreasing friction coefficient results from the larger debonding length. With a larger debonding length, the matrix in the cracked segment, which is under axial tension from the residual stresses, can contract more, which leads to an increase in crack-tip opening displacement and consequently in a higher stress intensity factor. It has to be noted that the results of the weight function method are considerably higher than those from the finite element calculations. This might be caused by the fact that the bridging stress profile used in the weight function method does not include the bending stresses found in the fibres in the finite element analysis.

Cyclic Fatigue

Figure 2: Comparison of crack-tip K_{max} from finite elements and weight function after an external load has been superposed on the thermal residual strains load for several friction coefficients.

In Fig.2, the K_{tip} recorded at maximum load is represented for both finite element and weight function method. Both sets of results show a reasonable agreement. Nevertheless, it has to be pointed out that the decrease of the crack-tip stress intensity factor is steeper for the weight function method. This is probably due to the constant frictional shear stress used in that analysis, compared to the variation of the frictional shear stress caused by Poisson contraction of the matrix, which affects Eqn.1 used in the finite element calculations. For all friction coefficients, the crack-tip stress intensity factor decreases with the increase in the number of bridging fibres during crack growth. Higher friction coefficients produce a larger decrease of the crack-tip stress intensity factor. This is again due to the smaller debonding length and thus smaller thermal stress relaxation induced contraction of the matrix. For an applied stress intensity factor range of ΔK_{appl}=10MPa√m , a similar trend was found, but the magnitude of the change in crack-tip stress intensity factor was smaller. During the finite element analysis, K_{min} and K_{max} have been calculated and the local crack-tip stress intensity factor range, shown in Fig.3, has been derived. In Fig.3, it is clear that the crack-tip stress intensity factor range decreases strongly with the increasing number of bridging fibres during crack

growth. The difference between the different friction coefficients is much smaller than for the respective K_{max} and K_{min} values. Nevertheless, it can be seen that higher friction coefficients lead to a smaller stress intensity factor range. At $\Delta K=10MPa\sqrt{m}$, ΔK_{tip} decreases, but the reduction is smaller than for $\Delta K=20MPa\sqrt{m}$.
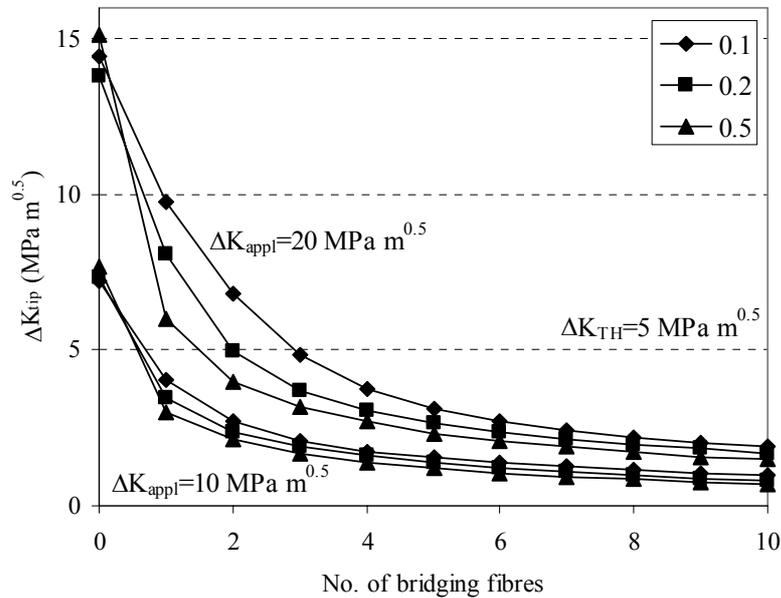
Figure 3: Crack-tip stress intensity factor range for two different applied load levels for friction coefficients of 0.1, 0.2 and 0.5.
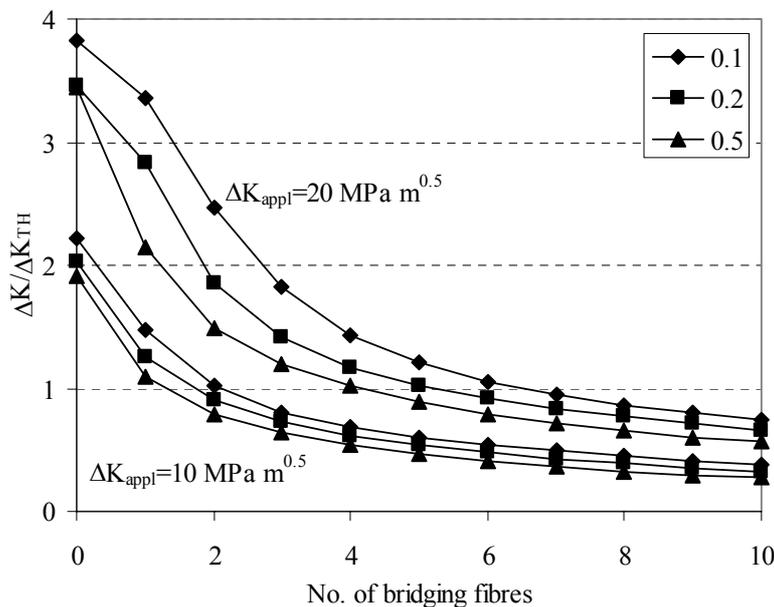
Figure 4: Crack growth criterion including the effect of the crack-tip load ratio on ΔK_{TH} for friction coefficients 0.1, 0.2 and 0.5.

For the applied external load, the load ratio R equals 0. For this load ratio, a threshold stress intensity factor $\Delta K_{TH}=5MPa\sqrt{m}$ has been reported for Ti-6Al-4V alloy [15]. Introducing this value into Fig.3, it can be inferred that for an applied load of $\Delta K=10MPa\sqrt{m}$, the crack would not progress beyond the first fibre, whereas for the load level of $\Delta K=20MPa\sqrt{m}$, the crack would progress only one or two fibres before crack arrest ($\Delta K/\Delta K_{TH}<1$). Crack growth is higher for lower friction coefficients. Due to the presence of thermal residual stresses and frictional interface shear stresses, the actual crack-tip load ratio is different from the applied load ratio. In fact, the crack-tip load ratio increases rapidly from between 0.2-0.4 towards a plateau

of approximately 0.8. By interpolating ΔK_{TH} values from [15] (ΔK_{TH}=4.6, 2.9 and 2.6 MPa√m for R=0.1, 0.5 and 0.8), the maximum crack extension can be calculated using the failure criterion $\Delta K/\Delta K_{TH}$. It can be seen in Fig.4 that by including the dependence of ΔK_{TH} on the crack-tip load ratio, crack arrest occurs at higher crack lengths compared to the values obtained for the load ratio R=0. For an applied stress intensity factor range of ΔK=10MPa√m, the crack would not grow beyond one or two fibres, depending on the friction coefficient. For a stress intensity factor range of ΔK=20MPa√m , the crack would not grow beyond 4 fibres for μ=0.5 and beyond 6 fibres for μ=0.1.

CONCLUSIONS

The analysis presented in this paper provides some important insights into the crack-tip stress intensity factors expected when frictional fibre bridging occurs during cyclic loading. It was found that in this fibre-reinforced composite, residual stresses arising from thermal expansion mismatch generate a crack opening load on the crack-tip in the absence of an applied load. This increase in the stress intensity factor is offset by the elastic transfer of load towards the fibres when an external load is applied so that $K_{tip} < K_{appl}$. For this reason, the bridging fibres produce a substantial reduction of the crack-tip stress intensity factor. With decreasing friction coefficient, the debonding length increases, which leads to an increase in the crack-tip stress intensity factor. In fact, relaxation of thermal stresses over longer debonding lengths leads to a more extensive matrix contraction locally, which results in a higher crack-tip stress intensity factor. It was found that under cyclic loading, the bridging mechanism is predicted to have a strong impact on crack growth. In fact, the high crack-tip shielding leads to crack arrest. Additionally, thermal residual stresses and fibre bridging have a strong impact on the crack-tip load ratio. Therefore, the variation of the fatigue threshold limit with the load ratio has to be incorporated into the crack growth criterion. Reasonable agreement has been found between the results from the finite element method and the weight function method.

REFERENCES

1. Venkateswara Rao, K.T., Siu, S.C. and Ritchie, R.O. (1993) Metallurgical Transactions 27A, 721-734
2. Cotterill, P.J. and Bowen, P. (1996) Mat. Sci. Tech. 12, 523-529
3. Barney, C., Ibbotson, A. and Bowen, P. (1998) Mat. Sci. Tech. 14, 658-668
4. Bao, G. and McMeeking, R.M. (1994) Acta Metall. Mater. 42, 2415-2425
5. Begley, M.R. and McMeeking, R.M. (1995) Comp. Sci. Tech. 53, 365-382
6. Ghosn, L.J., Kantzos, P. and Telesman, J. (1992) Int. J. Fract. 54, 345-357
7. Cox, B.N. and Lo, C. (1992) Acta Metall. Mater. 40, 1487-1496
8. Fett, T. (1994) KfK-Report 5291, Kernforschungszentrum Karlsruhe
9. Bao, G. and McMeeking, R.M. (1995) J. Mech. Phys. Solids 43, 1433-1460
10. Dinter, J., Peters, P.W.M. and Hemptenmacher, J. (1996) Composites 27A, 749-753
11. Ananth, C.R. and Chandra, N. (1996) Composites, 27A, 805-811
12. Zhao, D. and Botsis, J. (1996) Int. J. Fract. 82, 153-174
13. Tada, H., Paris, P.C. and Irwin, G.R. (1985) The stress analysis of Cracks Handbook, Del Research, St. Louis, MO
14. Withers, P.J. and Clarke, A.P. (1998) Acta Mater. 46, 6585-6598
15. Ritchie, R.O., Boyce, B.L., Campbell, J.P., Roder, O., Thompson, A.W. and Milligan, W.W. (1999) Int. J. Fatigue 21, 653-662